Effects of Debonding of PWAS on the Wave Propagation and the Electro-Mechanical Impedance Spectrum

Inka MUELLER [1], Alisa SHPAK [2], Mikhail V. GOLUB [2], Claus-Peter FRITZEN [1]

[1] University of Siegen, Institute of Mechanics and Control Engineering-Mechatronics
Paul-Bonatz-Strasse 9-11, 57076 Siegen, GERMANY
inka.mueller@uni-siegen.de, claus-peter.fritzen@uni-siegen.de
[2] Kuban State University, Institute for Mathematics, Mechanics and Informatics, Krasnodar 330040, RUSSIA
alisashpak7@gmail.com, m_golub@inbox.ru

Key words: piezoelectric wafer active sensors (PWAS), debonding, PWAS inspection, acousto-ultrasonics (AU), electro-mechanical impedance spectrum (EMI-spectrum)

Abstract

The use of piezoelectric wafer active sensors (PWAS) for acousto-ultrasonics (AU)-based structural health monitoring (SHM) purposes is state of the art. This paper deals with these piezoelectric transducers and aims to analyze their performance in case of defects of the PWAS itself. It focuses on the partial debonding of PWAS from the structure. Effects on the generated wave and the electro-mechanical impedance (EMI) spectrum are studied for a disc-shaped transducer with wrap-around electrode. The results show a dependency on the location of the debonded area in relation to the wrap-around electrode. Moreover, a high dependency on the excitation frequency is detected. The relevance for SHM purposes is shown by the analysis of the effects on a simple damage indicator, used for structural damage detection. Possibilities to detect this PWAS defect based on the EMI spectrum are presented.

1 INTRODUCTION

Acousto ultrasonics is an emerging field in the group of active SHM systems. Guided waves, which are excited in a structure, interact with damages. This interaction makes it possible to detect and even localize damages in structures. For many applications of acousto ultrasonic-based SHM systems, piezoelectric wafer active sensors (PWAS) are deployed. They can be used as sensors and actuators. This enables the data acquisition in a round robin fashion where consecutively one transducer is used as actuator and the others in turn as sensors. Simple disc-shaped transducers with a wrap-around electrode are easy to attach to the structure and comparably cheap. Embedded piezoelectric transducers, which can also be co-bonded to CFRP or GFRP structures, exist and enable the use of PWAS in uncomfortable surroundings.

To ensure a good performance of the SHM system, a reliable operation of the PWAS itself has to be secured. Several possible types of failure of the attached PWAS, like breakage of the transducer, degradation of the adhesive layer, degradation of the PWAS itself and debonding of the PWAS, exist. Different authors have already discussed these failure modes [1,2,3,4].

This paper focuses on the partial debonding of PWAS from the structure, based on experimental investigations. It is important to understand the effects on the wave

propagation, which are caused by these failures, to be able to cope with them. Moreover methods to detect these failures are mandatory.

To study the effects of debonding on the wave propagation, a laser Doppler vibrometer (LDV) is used. With its help the out-of-plane velocity component of the generated wave field is analyzed. The results for the generated wave field show a dependency on the location of the debonded area in relation to the wrap-around electrode as well as a relation to the excitation frequency. The effect for an SHM system is shown via analyzing the effects on a simple structural damage indicator. The LDV is also used to show the vibration of the debonded part of the transducer.

The detection of PWAS failure like debonding is possible with the help of the susceptance spectrum as a part of the electro-mechanical impedance spectrum. The effects of debonding on the susceptance spectrum are shown, before these measurements are used to show the performance of two methods of PWAS inspection, one already established [5] and one on the way to successful establishment, which has been presented in previous papers by the authors [6].

2 METHODS

For the analysis of the generated wave field and the EMI-spectrum of a debonded transducer different methods and equipment are used. They are shortly introduced in this section, giving necessary references for those methods.

For the description of the wave field a LDV is used to measure the out-of-plane velocity component. If this velocity is measured at a grid of points over an area, the vibration at a certain time can be visualized, as the velocity is the time derivative of the displacement resulting in similar patterns. Moreover, time lines of the velocity at different points are analyzed for describing the effect of debonding on the wave field. It is assumed, that they can be used as representative quantity for the measurement values of sensing transducers at specific points. They are used for the analysis of the effects of debonding on the results of an SHM system. Exemplary velocity signals, varying with time, for the undamaged and debonded case are shown in figure 1a).

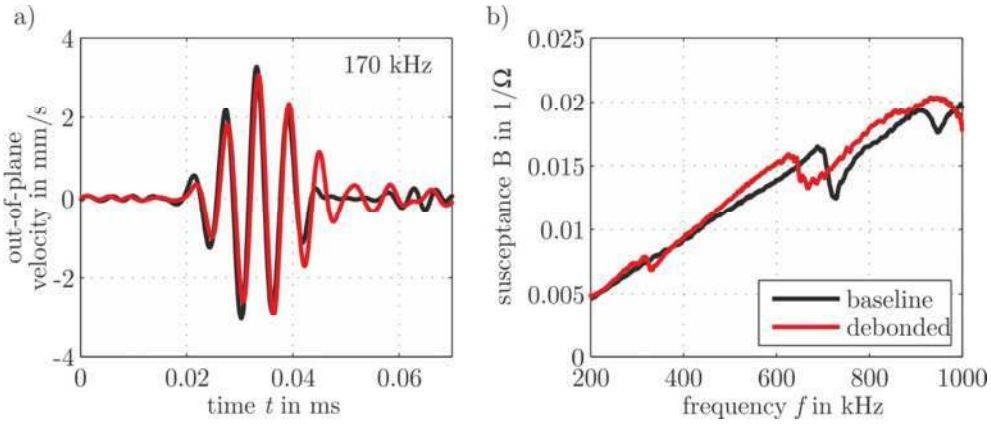

Figure 1: a) Out-of-plane velocity over time at an exemplary point for the baseline and the debonded case, b) exemplary susceptance spectra for a debonded and a fully bonded transducer.

For this investigation, a different simple SHM algorithm for structural damage detection has been defined, which is introduced here. For an overview of simple and advanced algorithms for structural damage detection the reader is referred to [7,8,9].

The structural damage indicator SDI_{RMS} uses the root-mean-square value for the difference signal between baseline y^H and new data y^D, weighted with the RMS value of the baseline. For the new signal y^D with time steps i from 1 to n this leads to:

$$SDI_{RMS} = \sqrt{\frac{\sum_{i=1}^{n}\left(y_i^D - y_i^H\right)^2}{\sum_{i=1}^{n}\left(y_i^H\right)^2}} \tag{1}$$

With the help of this damage indicator, which is a very simple approach for an SHM system for structural damage detection, the effect of the debonding on the SHM system will be analyzed.

For the identification of defect transducers in SHM systems, the EMI spectrum has proven to be a useful physical quantity. For many approaches the susceptance spectrum B as the imaginary part of the admittance spectrum, which is the reciprocal of the impedance spectrum, is used. Exemplary spectra are shown in figure 1b).

The susceptance of an unbound transducer is dominated by the capacitance C. The shape of the transducer, its bonding to the structure as well as the structure itself have an influence on the spectrum. Analytical models describing the susceptance exist, an overview is given in [10], a model, which focuses the transducer and its bonding line has been developed in [11].

Different methods on how to evaluate the susceptance exist. In this work, two methods are used and compared. The first method has been introduced by Park et al. [5]. It is based on the evaluation of the susceptance slope. Here, a slope coefficient SC for a given frequency interval is calculated, using a regression line. A change of the slope coefficient indicates a defect of the transducer. As frequency interval, a comparably low frequency range below the first eigenfrequency is chosen. Especially for damages, where a reduction of the active area of the transducer is present, this method shows very good results, as the reduction of the active area of the transducer leads to a decrease of the capacitance C. Nevertheless other PWAS defects can also be detected.

The second method uses a larger frequency interval for the comparison of baseline and new spectrum. In [6] it has been shown that some types of PWAS defects mainly lead to a change of the eigenfrequencies, visible in the susceptance spectrum, while the slope only experiences minor changes. Therefore a spectrum including the first eigenfrequency is compared, using the correlation coefficient CC. It is based on the covariance matrix $\boldsymbol{V}$ of the two susceptance spectra B^H and B^D.

$$CC = V_{12} \cdot (V_{11} \cdot V_{22})^{-1} \qquad DI_{CC} = 1 - |CC| \tag{2}$$

Due to the general positive trend of the susceptance over the frequency spectrum the influence of the slope on this PWAS damage indicator DI_{CC} is negligible.

3 EXPERIMENTAL RESULTS

3.1 Experimental Setup

The PWAS defect type, debonding, is analyzed with an experimental setup of 16 circular transducers of type PIC151 on an aluminum plate with dimensions of 500 mm x 500 mm x 2 mm. The transducers have a thickness of 0.25 mm and a diameter of 10 mm. Four transducers are fully bonded (PWAS 1-4), all other transducers are partially debonded. The

debonding is induced by the use of teflon foil, which prevents the adhesive layer to fully cover the PWAS-structure interface. The foil is removed after the bonding process is finished. Four partially debonded PWAS exhibit a debonded area of approx. 20%, which is consistent with a width of the debonded area of 1/4 of the diameter (PWAS 5-8). Four transducers are 50% debonded (PWAS 9-12) and four transducers are 80% debonded (PWAS 13-16). The orientation of the debonded area in relation to the location of the wrap-around electrode has been changed. The complete sample with all transducers is depicted in figure 2b). The orientation of the wrap-around electrode is fixed for all transducers in the west "W", as depicted in figure 2b) for PWAS 1. For each transducer the wave field can be analyzed with the LDV. A CLV1000 controller from Polytec was used with a CLV800 laser unit and a CLV700 measurement head. The head is mounted on a table with two moving axes. They are controlled via Matlab with a C11-4 motor controller from Isel. The measurements are collected and transferred to Matlab with a TiePie Engineering measurement device, called HS3. The equipment and experimental setup is depicted in figure 2a). It has to be taken into account that the transducers have different distance to the edges of the sample plate, resulting in different reflections. Therefore, only the direct signal without any signals reflected by the edges of the plate are used for the evaluation.

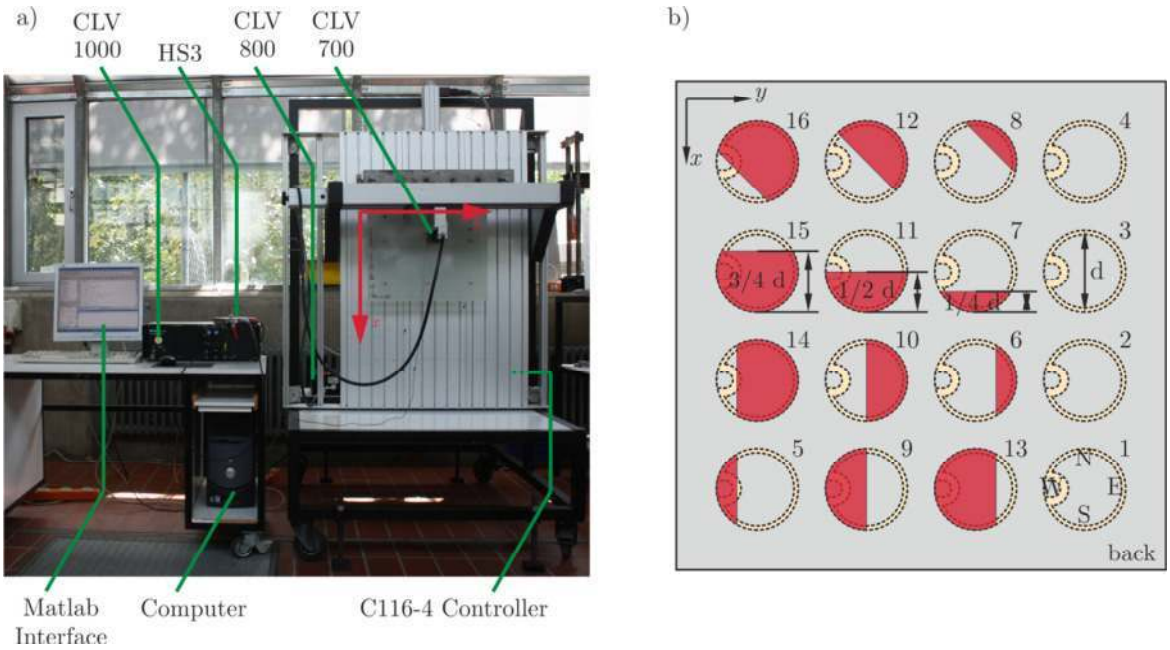

Figure 2: a) Experimental setup with a laser Doppler vibrometer head (CLV700) and necessary equipment, b) setup of the measured sample plate with 16 transducers, which have been bonded with different extent.

For the wave field two different types of measurements have been performed. For all transducers the out-of-plane velocity is measured at a distance of 20 mm in a circle around the PWAS center. The measurements points are located on the dotted circle, shown in figure 3c). Additionally, the generated wave field has been measured on the surface of the PWAS from the front for selected transducers. The different orientations of the sample for the measurement at the front and at the back of the sample are depicted in figure 3.

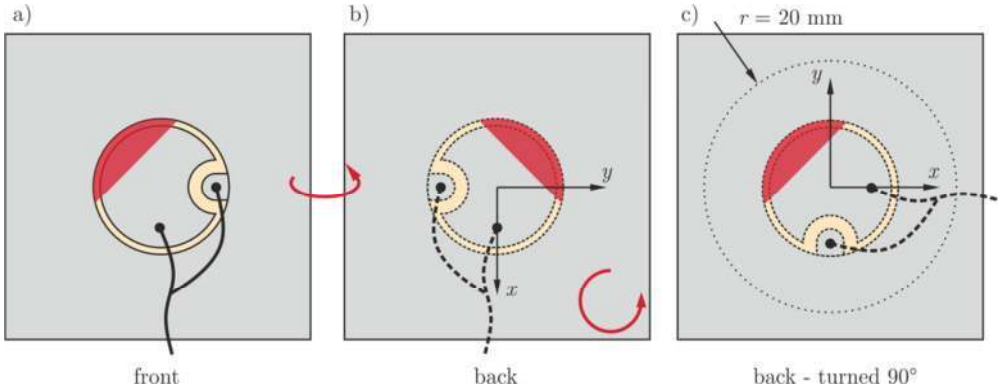

Figure 3: Different orientations of the measurement sample and LDV measurement locations

The impedance spectrum has been measured with the PZT Inspector, a measurement device for the wave propagation and EMI analysis of PWAS-based SHM systems, developed at the University of Siegen. Up to 32 channels can be measured subsequently within one experimental setup, allowing a low-cost automatic measurement of multiple channels. A detailed description is given by Fritzen et al. [12].

3.2 Analysis of the generated wave field

Before analyzing the generated wave field it has to be mentioned that the generated wave field of the fully bonded transducers is not axisymmetric. This is caused by the wrap-around electrode. It has been oriented in the west, as depicted in figure 2b) for PWAS 1, for all PWASs. This effect has already been described by Moll et al. [13]. The generated wave field has been measured at various points at a circle around the transducer from the back of the plate. The signals for two exemplary points at different central frequencies are depicted in figure 4 for the debonded (PWAS 8) and the fully bonded transducer.

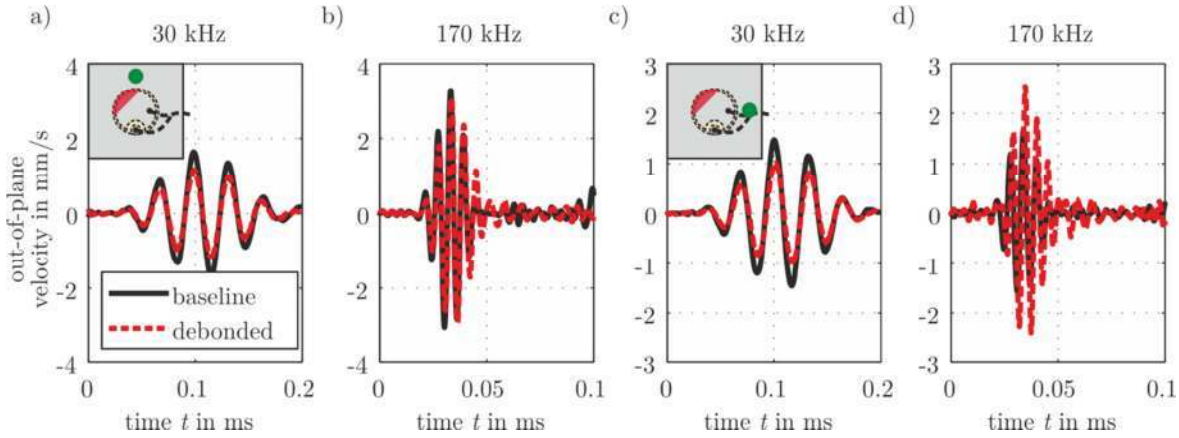

Figure 4: Out-of-plane velocity at two exemplary points for the baseline and debonded case for different excitation frequencies. The effect of debonding depends on the location and frequency.

The first point is opposite to the wrap-around electrode and 45° to the symmetry line of the defect. The second point is rotated 90° clockwise about the center of the PWAS compared to the first one as well as to the wrap-around electrode and 135° to the symmetry line of the defect. They are marked in figure 4a) and 4c).

For the first point the out-of-plane velocities, excited at central frequencies of 30 kHz and 170 kHz are shown in figure 4a) and b) for the fully bonded and defect case. For both central

frequencies a reduction of the maximum velocity amplitude is visible. Especially for 170 kHz, additional vibration after the decay of the input signal is visible for the debonded cases. Due to the location of the PWAS on the structure it can be assured that these vibrations are caused by the debonded PWAS and are not caused by additional reflections from edges of the structure. For the second point the time series for equivalent frequencies are shown in figure 4c) and 4d) for the fully bonded and defect case. For this point the debonding does not lead to a decrease of velocity amplitude for both frequencies. For 170 kHz an increase of amplitude is visible, caused by the debonding defect. The shift and rotation of the characteristic velocity field leads to these results. Moreover figure 4d) shows that the phase difference between the debonded and the fully bonded case exhibits a change from the beginning till the decay of the input signal. This might not be caused by a phase difference but by a change of the carrier frequency, see [14].

The additional vibration, shown in figure 4b) and 4d), is caused by energy trapping and localization in the debonded part. The visualization of the velocity field, measured at the surface of the PWAS, confirms this statement. In figure 5a) the velocity distribution at a single time step is displayed. The selected time is more than 2.5 times larger than the length of the input signal. For the fully bonded transducer the input signal has decayed. It has been secured that no reflections have returned to the PWAS yet. Nevertheless the debonded part is still vibrating.

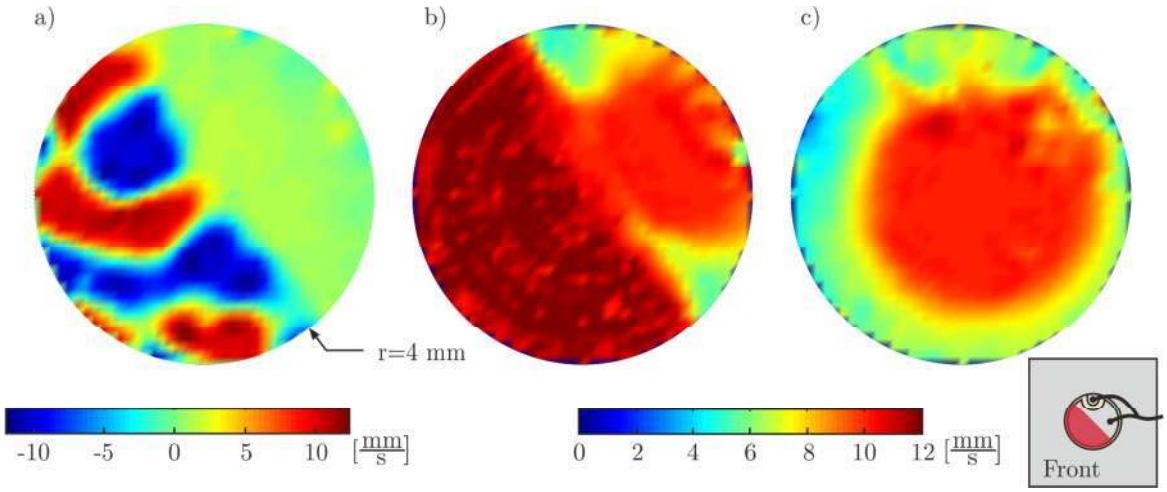

Figure 5: a) Distribution of out-of-plane velocity over the area of the PWAS measured from the front, a) distribution at a fixed time measured at a debonded transducer, b) distribution of the maxima of the velocity measured at a debonded transducer, c) distribution of the maxima of the velocity measured at a fully bonded transducer.

Figure 5b) and 5c) show the maxima of the velocity for the debonded and fully bonded transducer. As the velocity is measured at the top surface, the debonded part shows much higher amplitudes than the bonded part of the debonded transducer. Compared to the debonded case the velocity field for the undamaged PWAS is very symmetric, although minor deviations are visible at the location of the wrap-around electrode and at the second soldering point.

Summarizing, for different frequencies, debonding locations, PWAS orientations and sensing locations the effect of PWAS debonding on AU-based SHM is highly different.

Using the data of all transducers, it is possible to evaluate the structural damage indices for specific points. As the debonding is introduced during the bonding process, no baseline

measurement from exactly the same transducer is available. It is therefore necessary to use the baseline from another transducer. For all transducers PWAS 1 was used as baseline.

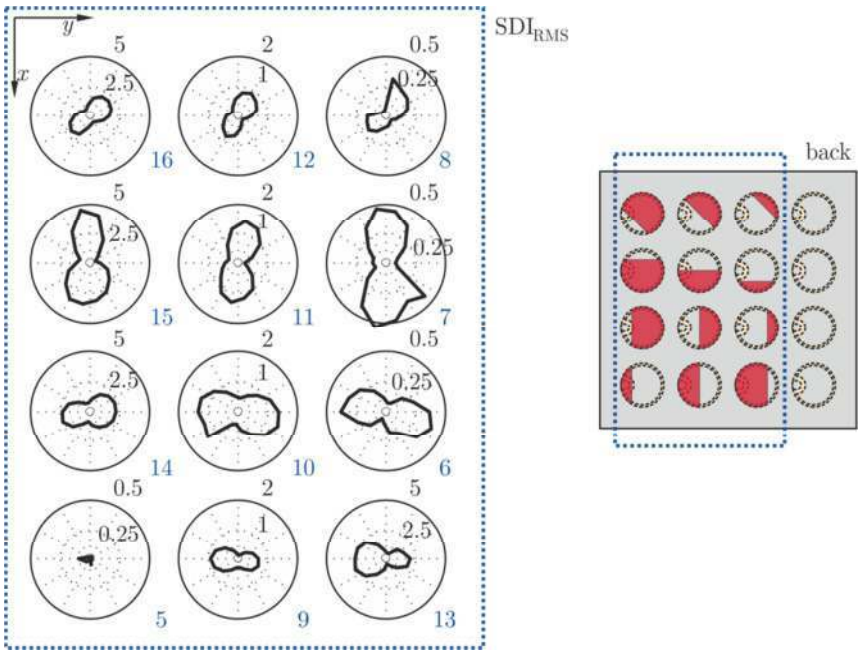

Figure 6: Evaluation of SDI_{RMS} for 12 PWAS with different orientation and extent of debonding for different angles. The effect of debonding on the structural damage indicator depends on the orientation and extent of the debonded area.

The values of SDI_{RMS} are depicted in polar plots for all debonded transducers in figure 6. The values show a high angular dependency. The pattern consists of two main lobes resulting in a peanut shape. This pattern is oriented according to the location of the debonding. All transducers with a debonding rate of 20% are depicted with a maximum structural damage index of 0.5, 50% with a maximum of 2 and 80% debonding with a maximum of 5, to show the similar pattern for all defect sizes. Compared to the other cases with 20% debonding, SDI_{RMS} is very small for the case of debonding directly under the wrap-around electrode. The pattern of SDI_{RMS} is oriented with its main axis from north to south "N" – "S", if the debonding is located in the south. This statement can be adopted for all other debonding orientations.

3.3 Analysis of the EMI spectra

The measured susceptance spectra for the four different stages, undamaged, 20% debonding, 50% debonding and 80% debonding are depicted in figure 7. The measurements are recorded at ambient temperature. For the debonded PWAS, an additional resonance can be found between 200 kHz and 350 kHz. Its characteristics are more pronounced with increasing debonding. A shift of the original resonance towards lower frequencies is visible and its features are less pronounced. For the highest debonding rate the new resonance is split into several similar frequencies. With increasing debonding size the trend of a higher slope in the low frequency range up to 150 kHz can be recognized, although a regression line over the whole frequency range from 100 kHz to 900 kHz will lead to similar results for the debonded and undamaged case.

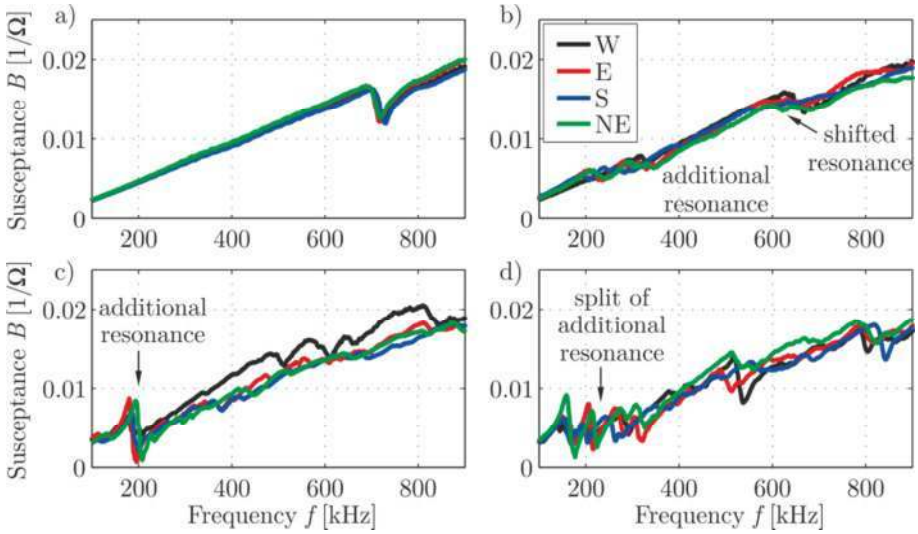

Figure 7: Susceptance spectra for 16 different transducers, a) fully bonded PWAS, b) 20% debonded PWAS show two resonances, c) 50% debonded PWAS, d) 80% debonded PWAS

The susceptance spectra can be used to calculate the two damage indices for PWAS defects, introduced in section "methods", slope coefficient *SC* and correlation coefficient based damage indicator DI_{CC}. As no baseline is available, similar to the wave propagation analysis, the susceptance spectrum of PWAS 1 is used as baseline for the calculation of DI_{CC}. Due to the different distance to the edges of the plate this leads to additional uncertainty in the data. For the calculation of *SC* no baseline is necessary. Nevertheless, data has to be compared to some reference value, here PWAS 1 can be used.

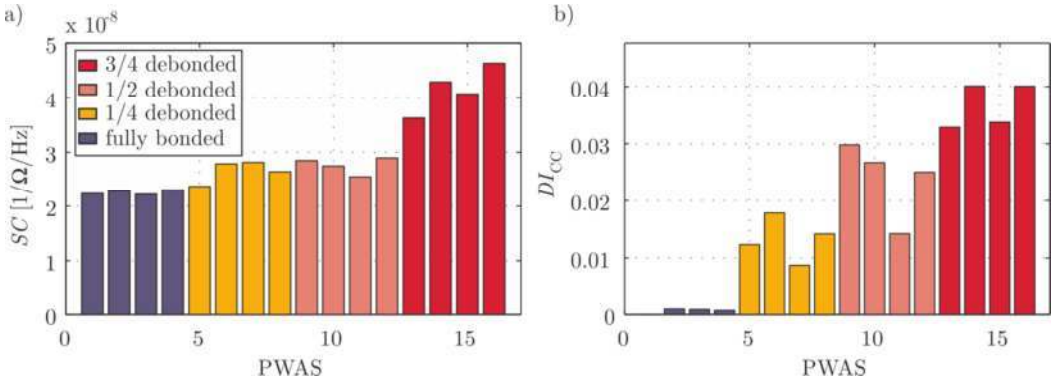

Figure 8: Evaluation of damage indicators to find damages of the PWAS, evaluated for all 16 PWAS using PWAS 1 as baseline, a) slope coefficient *SC*, b) correlation coefficient based indicator DI_{CC}.

The results for *SC* and DI_{CC} are shown in figure 8. The slope coefficient is evaluated in a frequency range from 40 kHz to 150 kHz. All debonded transducers show an increase of the susceptance slope, compared to the first values from the fully bonded transducers. Depending on the orientation of the debonded area the differences to the undamaged state are quite small - factor 1.06 for the smallest value of a defect transducer. The highest debonding rate of 80% can be clearly separated from the undamaged state, exhibiting a significantly increased slope coefficient.

As no baseline measurement from exactly the same transducer is possible, PWAS 1 was used as baseline for all transducers. This is possible, as all transducers ought to be the same and are bonded to the same continuous structure using the same procedure. Nevertheless, this

introduces some error and reduces the sensitivity of this method. The value of the damage index DI_{CC} for the other undamaged transducers gives an estimation on the error that is introduced to the calculation of DI_{CC} by this use of a baseline from another transducer.

All debonded transducers show an increased damage index DI_{CC}, which can be clearly separated from the undamaged state, see figure 8b). The calculated damage indices for the fully bonded transducers are much smaller than the smallest damage index of a debonded transducer, approx. by factor 10. The different orientations of the debonding lead to different levels of the damage index. “NE” and “E” are not located very close to the wrap-around electrode. Both show similar results and their damage indices are higher than those of “W” and “S”. An exception is the 50% debonding west, which shows higher damage indices than the other three locations for this state.

For the inspection of PWAS to find debonded transducers, DI_{CC} has proven to be a feasible quantity. For large debonded areas the slope coefficient SC is an alternative procedure to identify debonded transducers.

4 DISCUSSION

A debonding of PWAS leads to changes in its susceptance spectrum. These changes are dependent on the area of debonding and its location in relation to the wrapped electrode. The analysis of the impedance spectra showed that it is possible, to identify debonding with specific damage indicators for PWAS inspection. This enables an automated analysis of the data, which is absolutely necessary for the use in an automated SHM system check.

The effects of the PWAS defect “debonding” are non-negligible for the generated wave field. The time signals already reveal differences. These differences are highly angular and frequency dependent. The analysis indicates that this dependency is similar for damage indicators, used for SHM systems.

Depending on the sensitivity of the SHM system, these effects on the generated wave field already lead to false alarm. In the first place, it is not possible with this data to decide, whether the PWAS inspection method is able to identify the debonding, before it leads to false alarm of the SHM system. For this analysis it is definitely necessary to combine the results of the SHM system with the results of the PWAS inspection method. A possible method for this combination, which is based on statistics and probability of detection, has been presented by the Buethe and Fritzen in [15]. For this analysis thresholds and procedures of both methods for structural damage detection and for PWAS inspection have to be taken into account.

5 CONCLUSION

In this paper the effects of partial debonding of PWAS on the generated wave field, AU-based SHM system output and impedance spectra have been shown for a disc-shaped transducer with wrap-around electrode. Additionally to the extent of the debonding, other factors influence the effect. A dependency on the location of the debonded area in relation to the wrap-around electrode can be found. Moreover, the effects depend on the excitation frequency. The relevance for SHM purposes is shown by the analysis of the effects on a simple damage indicator, used for structural damage detection. To detect defect transducers, two different methods, based on the EMI spectrum have been used and compared, showing that it is possible to detect debonding with the help of the susceptance spectrum. For its use it is still necessary to verify the sensitivity, possible methods are mentioned in the discussion of the results.

ACKNOWLEDGEMENT

The experimental procedure is based on prior experiments by Dr. Jochen Moll, now Goethe University in Frankfurt. His help is very much appreciated and acknowledged.

REFERENCES

[1] Mulligan, K. R.; Quaegebeur, N.; Masson, P.; Brault, L.-P. & Yang, C., Compensation of piezoceramic bonding layer degradation for structural health monitoring, *Structural Health Monitoring*, **13**, 68-81, 2014.

[2] Gall, M.; Thielicke, B. & Schmidt, I., Integrity of piezoceramic patch transducers under cyclic loading at different temperatures, *Smart Materials and Structures*, 18, 104009, 2009.

[3] Blackshire, J. L.; Giurgiutiu, V.; Cooney, A. & Doane, J., Characterization of Sensor Performance and Durability for Structural Health Monitoring Systems, *Air Force Research Lab Technical Report*, 2005.

[4] Buethe, I. & Fritzen, C.-P., Investigation on Sensor Fault Effects of Piezoelectric Transducers on Wave Propagation and Impedance Measurements, *Proceedings of the Comsol Conference*, Rotterdam, 2013.

[5] Park, G.; Farrar, C. R.; di Scalea, F. L. & Coccia, S., Performance assessment and validation of piezoelectric active-sensors in structural health monitoring, *Smart Materials & Structures*, 15, 1673-1683, 2006.

[6] Buethe, I.; Moix-Bonet, M.; Wierach, P. & Fritzen, C.-P., Check of Piezoelectric Transducers Using the Electro-Mechanical Impedance, *Proceedings of the 7th EWSHM*, Nantes, 2014.

[7] Ostachowicz, W.; Kudela, P.; Krawczuk, M. & Zak, A., *Guided Waves in Structures for SHM - The Time-Domain Spectral Element Method*, Wiley, 2012.

[8] Farrar, C. & Worden, K., *Structural Health Monitoring: A Machine Learning Perspective*, Wiley, 2012.

[9] Su, Z. & Ye, L. *Identification of Damage Using Lamb Waves : From Fundamentals to Applications*, Springer, 2009.

[10] Giurgiutiu, V. *Structural Health Monitoring: with Piezoelectric Wafer Active Sensors*, Elsevier Science, 2nd edition, 2014.

[11] Buethe, I.; Eckstein, B. & Fritzen, C.-P. Model-based detection of sensor faults under changing temperature conditions, *Structural Health Monitoring*, 13, 109-119, 2014.

[12] Fritzen, C.-P.; Moll, J.; Chaaban, R.; Eckstein, B.; Kraemer, P.; Klinkov, M.; Dietrich, G.; Yang, C.; Xing, K. J. & Buethe, I., A Multifunctional Device for Multi-channel EMI and Guided Wave Propagation Measurements with PWAS, *Proceedings of the 7th EWSHM*, Nantes, 2014.

[13] Moll, J.; Golub, M. V.; Glushkov, E.; Glushkova, N. & Fritzen, C.-P., Non-axisymmetric Lamb wave excitation by piezoelectric wafer active sensors, *Sensors and Actuators A-physical Journal*, 174, 173-180, 2012.

[14] Golub, M. V.; Buethe, I.; Shpak, A. N.; Fritzen, C.-P.; Jung, H. & Moll, J., Analysis of Lamb Wave Excitation by the Partly Debonded Circular Piezoelectric Wafer Active Sensors, *11th European Conference on Non-Destructive Testing – ECNDT 2014*, Prague, 2014.

[15] Buethe, I. & Fritzen, C.-P., Quality Assessment for the EMI-based Inspection of PWAS, *Proceedings of the 10th IWSHM*, Stanford, 2015.